Latin American Journal of Solids and Structures
www.lajss.org

A Study on Acoustic Behavior of Poroelastic Media Bonded between Laminated Composite Panels

Abstract

A study on the acoustic behavior of double-walled panels, with sandwiched layer of porous materials is presented within Classical Laminated Plate Theory (CLPT) for laminated composite panels. For this purpose, equations of wave propagation are firstly extracted based on Biot's theory for porous materials, then the transmission loss (TL) of the structure is estimated in a broadband frequency. Secondly, TL coefficient of the structure is determined using Statistical Energy Analysis (SEA). In the next step, accuracy of the solution is shown with comparing the data obtained from these two presented models as well as the experimental results available in literature. Finally, the effects of parameters on sound transmission loss of double porous composite panels, especially at a high frequency range, are discussed. In addition, the results show that maximum sound energy is transferred through the waves frame (structure born) due to the porous layer bonded between the two composite panels. Therefore, material parameters that are principally related to solid phase of the foam such as Poisson's ratio, bulk density and bulk Young's modulus, have the most significant effects on the transmission loss. Meanwhile, the impacts of composite material panels and composite plies arrangement on sound transmission loss structures have been addressed in this paper.

Keywords

Laminated Composite Panels, Sound Transmission Loss, Porous, Biot's theory, Statistical Energy Analysis (SEA).

Mohammad Hassan Shojaeefard [a, c]
Roohollah Talebitooti [b, c, *]
Reza Ahmadi [d]
Behzad Ranjbar [e]

[a] Prof., Sch. of Mech. Eng., Iran Univ. of Sci. and Tech., Iran, mhshf@iust.ac.ir
[b] Asst. Prof., Sch. of Mech. Eng., Iran Univ. of Sci. and Tech., Iran, rtalebi@iust.ac.ir.
[c] Automotive Simulation & Optimal Design Research Lab., Sch. of Auto. Eng., Iran Univ. of Sci. and Tech., Tehran, Iran.
[d] PhD. Stu., Sch. of Auto. Eng., Iran Univ. of Sci. and Tech., Iran, rahmadi@auto.iust.ac.ir
[e] MSc., Sch. of Auto. Eng., Iran Univ. of Sci. and Tech., Iran, branjbar@auto.iust.ac.ir
* Author email: rtalebi@iust.ac.ir

Received 24.12.2013
In revised form 30.06.2014
Accepted 30.06.2014
Available online 17.08.2014

Nomenclature

A_{ij}	Extensional stiffness in composite panel	(x, y, z)	Components of global Cartesian coordinate
A_p	Area of the panel	α_∞	Tortuosity
b	Viscous coupling factor	γ	Angle of incidence
B_{ij}	Coupling stiffness in composite panel	δ	Shear modulus of the porous material
c_2	Speed of sound in the fluid phase	$\{\varepsilon^{(0)}\}$	Membrane strain
c_3, c_1	Speed of sound in external and cavity medium	$\{\varepsilon^{(1)}\}$	Flexural (Bending) strain
D_{ij}	Bending stiffness in composite panel	ζ_i	Potential function of incident plane
E	Bulk Young's modulus of the solid phase	η_{ij}	Coupling loss factor
e_s	Solid volumetric strain	$\{\lambda\}$	Vector showing the unknown parameters
h_p	Thickness of the panel	ν	Poisson's ratio of the solid phase
h_{foam}	Thickness of the porous layer	ξ	Wave number
$\{H\}$	Vector representing the acoustic forces	ξ_x, ξ_y	Wave numbers in x and y direction
$[\hbar]$	Coefficient matrix	Π_i^{diss}	Power dissipated in ith system
I_0 , I_1	Mass moments of inertia	Π_i^{in}	Power input to ith subsystem
j_0 , j_1	Bessel functions of the first type with zero and first orders	Π_{ij}	Power flow between subsystems i and j
k_v	Air viscosity	Π_{inc}	Sound power incident on the dividing partition of area in the source room
M_{ij}	In-plane moment resultants	$\overline{\omega}$	Rotational strain
N_{ij}	In-plane force resultants	ρ^*	Surface density
n_i	Modal densities of subsystem i	$\rho^{(k)}$	Density of the panel at kth layer
P	Pressure in the exterior acoustics field at the interface	ρ_0	Density of the fluid phase
Pr	Prandtl number	ρ_1	Bulk density of the solid phase
$< P_1^2 >$	Average square sound pressure	$\hat{\rho}_{11}$, $\hat{\rho}_{12}$, $\hat{\rho}_{22}$	Equivalent mass
P_{n1}^i	Acoustic pressures of the incident wave	ρ_{3a}, ρ_{1a}	Density in external and cavity medium
P_{n1}^R	Acoustic pressures of the reflected wave	ρ_a	Inertial coupling term
P_{n3}^T	Acoustic pressure of the transmitted wave	ρ_s	Density of the panel
q	Total transvers load	σ_r	Flow resistivity
$\overline{Q}_{ij}^{(k)}$	Function of physical properties of each ply (kth)	ς	Ratio of specific heat
TL_{avg}	Averaged Transmission Loss	$\tau_{(\gamma)}$	Ratio of amplitudes of the incident and transmitted waves
$\overline{u}$	Displacement vector of the solid phase	$\overline{\tau}$	Averaged pressure transmission coefficient
U_0 , V_0 , W_0	Displacements of the mid-plane	φ	Porosity
v	Velocity of the panel	χ , ϕ , μ	Elastic properties of the porous materials

V_1	Volume the cavity	ω	Angular frequency
V_y	Normal component of the particle velocity in the exterior medium at the interface	Λ	Viscous characteristic length
W_p^0, W_T^0	Transverse and shear waves for the panel	∇	Laplacian operator

1 INTRODUCTION

In recent years, the use of high-performance materials that have light weight and high stiffness, has been increasing in many fields of engineering. Laminated composites are becoming the materials of choice in various technical applications, including aerospace, mechanical, marine, and automotive engineering, due to their high strength-to-weight ratios. However, noise transmission through these structures especially at high frequencies is a critical issue, because it suffers from a low density. Therefore, to reduce the noise transmission, engineers try to apply the porous media as a layer between two composite panels.

There are a lot of theories that model porous materials with different approximate calculations. The most complete and sophisticated model to describe the equations of wave propagation in the porous layer is Biot's theory (Biot, 1956). This theory was presented on the basis of acoustic modeling of the porous materials where the solid phase was assumed without deformation. In other words, shear wave propagation through the solid phase was considered in these materials. Bolton et al. also presented a method based on the Biot's theory where the porous material was assumed to be a homogeneous material (Bolton and Green, 1993; Bolton et al., 1997). This theory has allowed all three waves to be propagated in the porous material. These waves include two longitudinal waves (frame and airborne waves) and one shear (rotational) wave. This method will be referred to as the full method hereafter.

Bolton and Kang interpreted the macroscopic properties of the porous materials (Bolton et al., 1996). They properly showed the powerful effects of the porous material as a sound insulation. Models of Allard and Atalla were initially developed to describe the wave propagation in the porous media saturated by heavy fluids (Allard and Atalla, 2009). Their model was used to predict acoustical performances of an air saturated sound absorbing porous media. Cimerman et al. proposed SEA model to simulate the sound behavior of vehicle subsystems as sound barriers (Cimerman et al., 1995). Xiandi Zeng et al. studied the effect of laminated steel body panels on sound pressure level inside a car (Zeng et al., 2002). They have also simulated the SEA model of a vehicle and then, compared transmission loss of the laminated panels with the conventional one. In addition, they have demonstrated that the laminated panels used in automotive comportments such as roof panel and front dash can reduce the noise from road and driveline. Tadeu et al. investigated the sound insulation features provided by single and double panels of steel, concrete and glass (Tadeu et al., 2004). Onsay proposed a SEA model to examine the corresponding issues such as improving the sound and vibration quality as well as decreasing the manufacturing costs (Onsay, 2007). Ghosh et al. have presented the experimental setup to show the effective performance of porous material as an insulator (Ghosh et al., 2008). Xin et al. have studied the vibration behavior of double-walled acoustic structures (Xin et al., 2008). They have also studied the transmission loss of orthogonal rib-stiffened double-panel structures (Xin and Lu, 2011). More recently, Daneshjou et al. have in-

vestigated acoustic properties of the double-layer composite cylindrical shells by applying porous media between the layers (Daneshjou et al., 2011).

A brief literature review clearly shows that, there is no investigation on acoustic transmission of double-walled laminated composites consisting of porous layers, although the transmission loss of these composite panels is critical to their applications. Thus, in this paper, a novel modeling of the acoustic transmission of laminated composite double-walled panels lined with porous materials is presented. Also Biot's theory (Biot, 1956) is used to model the wave propagation in porous layer which clearly account of all the 3 types of the wave propagation in elastic porous materials. Therefore, the equations of wave propagation are extracted based on this theory, considering viscous and inertia coupling in dynamic equation, as well as stress transfer, thermal and elastic coupling in stress-strain relationships of porous material and also vibration equations of composite layers. Solving these equations along with boundary conditions, simultaneously the transmission loss of a structure will be calculated. Then, the SEA method are developed to predict the sound power transmission through double composite panels lined with elastic porous media. The results from analytical calculations and the SEA modeling are compared with the experimental data. Finally, the influence of effective parameters of this structure on the transmission loss of the multilayer systems, will be studied particularly at high frequencies.

2 MODEL DESCRIPTION

A schematic view of a double-walled composite panel with an infinite length subjected to a plane wave of γ incidence angle is shown in Figure 1. The thicknesses of the panels are h_{p1} and h_{p2}. In addition, a concentric layer of the porous material is installed between the panels (h_{foam}). Moreover, the acoustic media inside and outside of the panel are represented by the speed of sound (c_1, c_3) and the density (ρ_{1a}, ρ_{3a}), respectively.

Thirteen types of wave branches are propagated into the structure including two incident and reflected waves (p_{n1}^{i}, p_{n1}^{R}), four waves in the composite plates (longitudinal and shear waves for the first plate (W_{p1}^{0}, W_{t1}^{0}) and the second one (W_{p2}^{0}, W_{t2}^{0}), three branches of transmitted as well as three reflected waves in the porous material (p_{n2}^{T1}, p_{n2}^{T2}, p_{n2}^{T3}, p_{n2}^{R1}, p_{n2}^{R2} and p_{n2}^{R3}) and finally a transmitted wave into the third medium (p_{n3}^{T}) as assumed to be an anechoic environment.

Assuming the two dimensional problem of wave propagation through a porous material, the potential function of incident plane wave with unit amplitude is written as (Bolton et al., 1996):

$$\zeta_i = e^{-j(\xi_x x + \xi_y y)} \tag{1}$$

where:

$$\xi_x = \frac{\omega}{c_1}\sin\gamma \tag{2}$$

$$\xi_y = \frac{\omega}{c_1}\cos\gamma \tag{3}$$

In the above equations, c_1 is the speed of sound in the incident medium, ω is the angular frequency, γ is the angle of incidence and j is the imaginary unit.

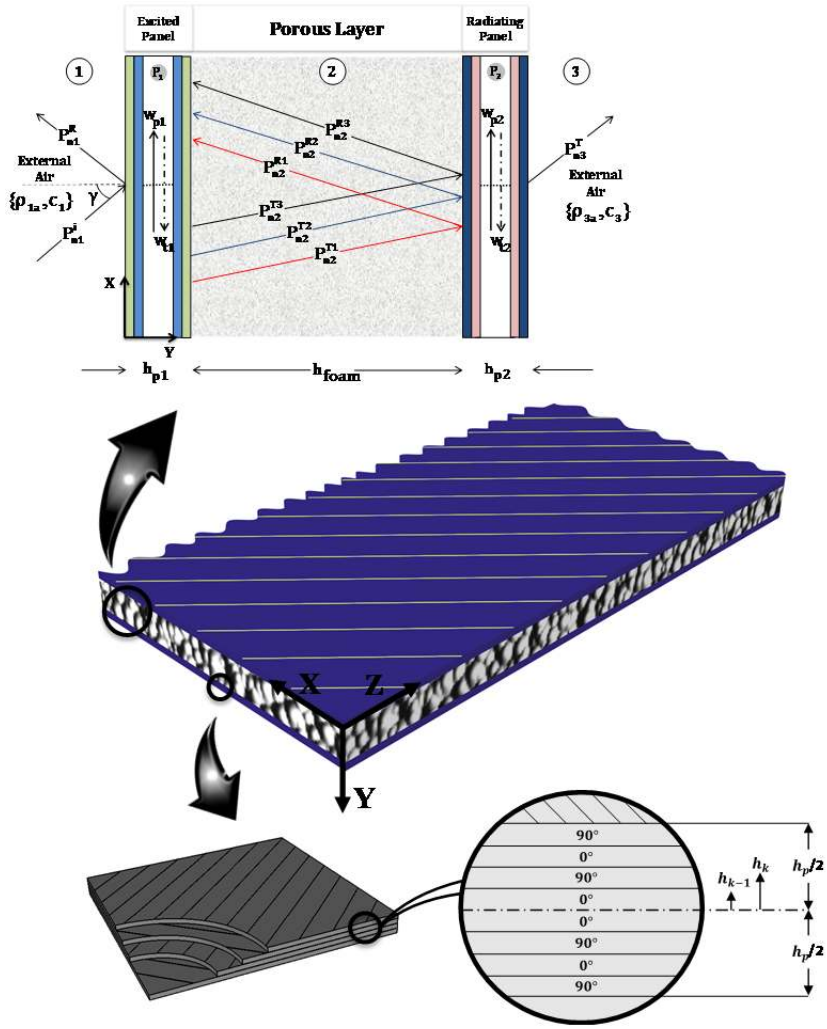

Figure 1: Wave propagation through composite panel.

3 ANALYTICAL FORMULATION

3.1 Dynamic Equations in Porous Medium

The equations presented in this section are used to relate the forces acting on an incremental volume to its resulting motion. For the solid phase in (x, y, z) directions, the following differential form of the equation of equilibrium is given (Bolton et al., 1996):

$$\frac{\partial \hat{\tau}_{xi}}{\partial x}+\frac{\partial \hat{\tau}_{yi}}{\partial y}+\frac{\partial \hat{\tau}_{zi}}{\partial z}=\rho_1\frac{\partial^2 \overline{u}_i}{\partial t^2}+\rho_a\frac{\partial^2}{\partial t^2}(\overline{u}_i-\overline{U}_i)+b\frac{\partial}{\partial t}(\overline{u}_i-\overline{U}_i) \quad @\, i=x,y,z \tag{4}$$

The force balance appropriate for the fluid phase is defined as follows:

$$\frac{\partial \hat{\sigma}^f}{\partial i}=\rho_0\varphi\frac{\partial^2 \overline{U}_i}{\partial t^2}+\rho_a\frac{\partial^2}{\partial t^2}(\overline{U}_i-\overline{u}_i)+b\frac{\partial}{\partial t}(\overline{U}_i-\overline{u}_i) \qquad @\, i=x,y,z \tag{5}$$

where $\overline{u}_i$, $\hat{\tau}_{ii}=\hat{\sigma}_i^s$ and $\hat{\tau}_{ij}$ are displacements and stresses in the solid phase, respectively. Moreover, $\overline{U}_i$ and $\hat{\sigma}^f$ are the displacements and the stresses in fluid phase, respectively.

In the above-mentioned equations, b denotes a viscous coupling factor, ρ_1 represents bulk density of the solid phase, ρ_0 is density of the fluid phase of the porous material and ρ_a is the inertial coupling term, presented by:

$$\rho_a=\rho_0\varphi(\alpha_\infty-1) \tag{6}$$

The following equation is used to calculate the coupling coefficient, b:

$$b=\varphi^2\sigma_r\sqrt{1+j\omega/H} \tag{7}$$

where the viscous characteristic frequency, H, is defined as follows (Bolton et al., 1996):

$$H=\sigma_r^2\Lambda^2\varphi^2/4\alpha_\infty^2 k_v\rho_0 \tag{8}$$

α_∞, k_v, Λ, σ_r and φ represent tortuosity, air viscosity, viscous characteristic length, flow resistivity and porosity, respectively.

3.2 Wave Equations in Porous Media

The porous material is assumed to be homogeneous and isotropic aggregate of the elastic frame. Then, with substituting stress-strain equations into the dynamic equations for the solid and fluid phases, Eq. (4) and Eq. (5), the acoustical behavior of the structure can be described by the following two wave equations (Bolton et al., 1996; Lee et al., 2001):

$$\nabla^4 e_s+A_1\nabla^2 e_s+A_2 e_s=0 \tag{9}$$

$$\nabla^2\overline{\omega}+\xi_4^2\overline{\omega}=0 \tag{10}$$

Eq. (9) and Eq. (10) determine two elastic longitudinal waves and one rotational wave, respectively. In the above equation, $e_s=\nabla.\overline{u}$ denotes solid volumetric strain ($\overline{u}$, is displacement vector of the solid phase) and $\overline{\omega}=\nabla\times\overline{u}$ denotes rotational strain. The parameters A_1 and A_2 are obtained as below:

$$A_1 = \frac{\omega^2}{(\phi\mu - \chi^2)}(\hat{\rho}_{11}\mu + \hat{\rho}_{22}\phi - 2\hat{\rho}_{12}\chi) \tag{11}$$

$$A_2 = \frac{\omega^4}{(\phi\mu - \chi^2)}(\hat{\rho}_{11}\hat{\rho}_{22} - \hat{\rho}_{12}{}^2) \tag{12}$$

The complex wave numbers of the two longitudinal waves ξ_α and ξ_β are obtained as:

$$\xi_\alpha{}^2 = (A_1 + \sqrt{A_1{}^2 - 4A_2}) / 2 \tag{13}$$

$$\xi_\beta{}^2 = (A_1 - \sqrt{A_1{}^2 - 4A_2}) / 2 \tag{14}$$

Moreover, the corresponding wave number of the shear wave, ξ_4, is given as:

$$\xi_4^2 = (\omega^2 / \delta)\ \left[\hat{\rho}_{11} - (\hat{\rho}_{12})^2 / \hat{\rho}_{22}\right] \tag{15}$$

In the above-mentioned equations, δ is the shear modulus of the porous material, while χ, ϕ and μ express the elastic properties of the porous materials. These are extensively explained in (Bolton et al., 1996; Lee et al., 2001). $\hat{\rho}_{11}$, $\hat{\rho}_{12}$ and $\hat{\rho}_{22}$ stand for equivalent masses:

$$\begin{aligned}
\hat{\rho}_{11} &= \rho_1 + \rho_a - j\sigma_r\varphi^2\left(\frac{1}{\omega} + \frac{4j\alpha_\infty^2 k_v\rho_0}{\sigma_r^2\Lambda^2\varphi^2}\right)\\
\hat{\rho}_{12} &= -\rho_a + j\sigma_r\varphi^2\left(\frac{1}{\omega} + \frac{4j\alpha_\infty^2 k_v\rho_0}{\sigma_r^2\Lambda^2\varphi^2}\right)\\
\hat{\rho}_{22} &= \rho_2 + \rho_a - j\sigma_r\varphi^2\left(\frac{1}{\omega} + \frac{4j\alpha_\infty^2 k_v\rho_0}{\sigma_r^2\Lambda^2\varphi^2}\right)
\end{aligned} \tag{16}$$

where:

$$\begin{aligned}
\phi &= A + 2\delta\\
A &= \frac{\nu\ E}{(1+\nu)(1-2\nu)}\\
\delta &= \frac{E}{2(1+\nu)}\\
\chi &= (1-\varphi)G\\
\mu &= \varphi G
\end{aligned} \tag{17}$$

Here E and ν are bulk Young's modulus and Poisson's ratio of the solid phase, respectively. Assuming that the pores are shaped in a cylindrical form, then G is expressed as:

$$G = \rho_0 c_2^2 \left\{ 1 + \frac{(\varsigma - 1)\sqrt{\varphi\sigma_r}}{\mathrm{Pr}^{\frac{1}{2}}\sqrt{-2j\omega\rho_0\alpha_\infty}} \frac{j_1\left(2\,\mathrm{Pr}^{\frac{1}{2}}\sqrt{\frac{-2j\omega\rho_0\alpha_\infty}{\varphi\sigma_r}}\right)}{j_0\left(2\,\mathrm{Pr}^{\frac{1}{2}}\sqrt{\frac{-2j\omega\rho_0\alpha_\infty}{\varphi\sigma_r}}\right)} \right\}^{-1} \tag{18}$$

where c_2, ς, Pr, j_0 and j_1 are the speed of sound in the fluid phase of the porous materials, the ratio of specific heat, the Prandtl number, the Bessel functions of the first type with zero and first orders, respectively. Assuming the wave propagation through porous material, the displacement and stress fields of the solid and fluid phases along x and y directions have been derived by Bolton et al. (Bolton et al., 1996).

The displacement components in solid phase of porous material are obtained as:

$$\begin{aligned} \hat{u}_x &= j\xi_x e^{-j\xi_x x}\left[\frac{p_{n2}^{T1}}{\xi_\alpha^2}e^{-j\xi_{\alpha y}y} + \frac{p_{n2}^{R1}}{\xi_\alpha^2}e^{j\xi_{\alpha y}y} + \frac{p_{n2}^{T2}}{\xi_\beta^2}e^{-j\xi_{\beta y}y} + \frac{p_{n2}^{R2}}{\xi_\beta^2}e^{j\xi_{\beta y}y}\right] \\ &\quad - j\frac{\xi_{4y}}{\xi_4^2}e^{-j\xi_x x}\left[p_{n2}^{T3}e^{-j\xi_{4y}y} - p_{n2}^{R3}e^{j\xi_{4y}y}\right] \end{aligned} \tag{19}$$

$$\begin{aligned} \hat{u}_y &= je^{-j\xi_x x}\left[\frac{\xi_{\alpha y}}{\xi_\alpha^2}p_{n2}^{T1}e^{-j\xi_{\alpha y}y} - \frac{\xi_{\alpha y}}{\xi_\alpha^2}p_{n2}^{R1}e^{j\xi_{\alpha y}y} + \frac{\xi_{\beta y}}{\xi_\beta^2}p_{n2}^{T2}e^{-j\xi_{\beta y}y} - \frac{\xi_{\beta y}}{\xi_\beta^2}p_{n2}^{R2}e^{j\xi_{\beta y}y}\right] \\ &\quad + j\frac{\xi_x}{\xi_4^2}e^{-j\xi_x x}\left[p_{n2}^{T3}e^{-j\xi_{4y}y} + p_{n2}^{R3}e^{j\xi_{4y}y}\right] \end{aligned} \tag{20}$$

The displacement components in fluid phase of porous material are followed as:

$$\begin{aligned} \hat{U}_x &= j\xi_x e^{-j\xi_x x}\left[b_1\frac{p_{n2}^{T1}}{\xi_\alpha^2}e^{-j\xi_{\alpha y}y} + b_1\frac{p_{n2}^{R1}}{\xi_\alpha^2}e^{j\xi_{\alpha y}y} + b_2\frac{p_{n2}^{T2}}{\xi_\beta^2}e^{-j\xi_{\beta y}y} + b_2\frac{p_{n2}^{R2}}{\xi_\beta^2}e^{j\xi_{\beta y}y}\right] \\ &\quad - jg\frac{\xi_{4y}}{\xi_4^2}e^{-j\xi_x x}\left[p_{n2}^{T3}e^{-j\xi_{4y}y} - p_{n2}^{R3}e^{j\xi_{4y}y}\right] \end{aligned} \tag{21}$$

$$\begin{aligned} \hat{U}_y &= je^{-j\xi_x x}\left[b_1\frac{\xi_{\alpha y}}{\xi_\alpha^2}p_{n2}^{T1}e^{-j\xi_{\alpha y}y} - b_1\frac{\xi_{\alpha y}}{\xi_\alpha^2}p_{n2}^{R1}e^{j\xi_{\alpha y}y} + b_2\frac{\xi_{\beta y}}{\xi_\beta^2}p_{n2}^{T2}e^{-j\xi_{\beta y}y} - b_2\frac{\xi_{\beta y}}{\xi_\beta^2}p_{n2}^{R2}e^{j\xi_{\beta y}y}\right] \\ &\quad + jg\frac{\xi_x}{\xi_4^2}e^{-j\xi_x x}\left[p_{n2}^{T3}e^{-j\xi_{4y}y} + p_{n2}^{R3}e^{j\xi_{4y}y}\right] \end{aligned} \tag{22}$$

The stress components in solid phase are written as:

$$\begin{aligned}\hat{\sigma}_y^s = e^{-j\xi_x x}[&(2\delta\frac{\xi_{\alpha y}^2}{\xi_\alpha^2}+A+b_1\chi)p_{n2}^{T1}e^{-j\xi_{\alpha y}y}+(2\delta\frac{\xi_{\alpha y}^2}{\xi_\alpha^2}+A+b_1\chi)p_{n2}^{R1}e^{j\xi_{\alpha y}y}\\&+(2\delta\frac{\xi_{\beta y}^2}{\xi_\beta^2}+A+b_2\chi)p_{n2}^{T2}e^{-j\xi_{\beta y}y}+(2\delta\frac{\xi_{\beta y}^2}{\xi_\beta^2}+A+b_2\chi)p_{n2}^{R2}e^{j\xi_{\beta y}y}\\&+2\delta\frac{\xi_{4y}\xi_x}{\xi_4^2}(p_{n2}^{T3}e^{-j\xi_{4y}y}-p_{n2}^{R3}e^{j\xi_{4y}y})]\end{aligned} \tag{23}$$

$$\begin{aligned}\hat{\tau}_{xy} = e^{-j\xi_x x}\delta[&2\frac{\xi_{\alpha y}\xi_x}{\xi_\alpha^2}(p_{n2}^{T1}e^{-j\xi_{\alpha y}y}-p_{n2}^{R1}e^{j\xi_{\alpha y}y})+2\frac{\xi_{\beta y}\xi_x}{\xi_\beta^2}(p_{n2}^{T2}e^{-j\xi_{\beta y}y}-p_{n2}^{R2}e^{j\xi_{\beta y}y})\\&+\frac{(\xi_x^2-\xi_{4y}^2)}{\xi_4^2}(p_{n2}^{T3}e^{-j\xi_{4y}y}+p_{n2}^{R3}e^{j\xi_{4y}y})]\end{aligned} \tag{24}$$

Finally, the stress of fluid phase is written as:

$$\begin{aligned}\hat{\sigma}^f = e^{-j\xi_x x}[&(\chi+b_1\mu)p_{n2}^{T1}e^{-j\xi_{\alpha y}y}+(\chi+b_1\mu)p_{n2}^{R1}e^{j\xi_{\alpha y}y}+(\chi+b_2\mu)p_{n2}^{T2}e^{-j\xi_{\beta y}y}\\&+(\chi+b_2\mu)p_{n2}^{R2}e^{j\xi_{\beta y}y}]\end{aligned} \tag{25}$$

where:

$$\begin{aligned}\xi_{iy} &= \sqrt{\xi_i^{\,2}-\xi_x^{\,2}} \qquad @\ i=\alpha,\beta,4\\ g &= -\hat{\rho}_{12}\,/\,\hat{\rho}_{22}\\ b_1 &= a_1-a_2\xi_\alpha^{\,2}\\ b_2 &= a_1-a_2\xi_\beta^{\,2}\\ a_1 &= \frac{\hat{\rho}_{11}\mu-\hat{\rho}_{12}\chi}{\hat{\rho}_{22}\chi-\hat{\rho}_{12}\mu}\\ a_2 &= \frac{\phi\mu-\chi^2}{\omega^2(\hat{\rho}_{22}\chi-\hat{\rho}_{12}\mu)}\end{aligned} \tag{26}$$

It is notable that six constants p_{n2}^{T1}, p_{n2}^{T2}, p_{n2}^{T3}, p_{n2}^{R1}, p_{n2}^{R2} and p_{n2}^{R3} have to be determined by applying the boundary conditions.

3.3 Wave Propagation through Laminated Composites

Due to power transmission, the composite panels are known as the media of wave propagation, and hence the equations of motion in the laminated composite panels are described here. The Classical Laminated Plate Theory (CLPT) is investigated in this contribution based on Kirchhoff Hypothesis (Reddy, 2004). In formulating the theory, certain assumptions or restrictions are made, as stated here (Reddy, 2004):

- The layers are perfectly bonded together (assumption).
- The material of each layer is linearly elastic and has three planes of material symmetry (restriction).

- Each layer is of uniform thickness (restriction).
- The strains and displacements are small (restriction).
- The transverse shear stresses on top and bottom surfaces of the laminate are zero (restriction).

So according to this theory, normal and transverse shear strains would be equal to zero:

$$\varepsilon_{yy} = \gamma_{xy} = \gamma_{zy} = 0 \tag{27}$$

The equations of motion in longitudinal (x), lateral (z), and thickness (y) directions of a laminated composite thin plate in Cartesian coordinate can be written as follows (Reddy, 2004):

$$\begin{aligned}
&\frac{\partial N_{xx}}{\partial x} + \frac{\partial N_{xz}}{\partial z} = I_0 \frac{\partial^2 U_0}{\partial t^2} - I_1 \frac{\partial^2}{\partial t^2}\left(\frac{\partial W_0}{\partial x}\right) \\
&\frac{\partial N_{xz}}{\partial x} + \frac{\partial N_{zz}}{\partial z} = I_0 \frac{\partial^2 V_0}{\partial t^2} - I_1 \frac{\partial^2}{\partial t^2}\left(\frac{\partial W_0}{\partial z}\right) \\
&\frac{\partial^2 M_{xx}}{\partial x^2} + 2\frac{\partial^2 M_{xz}}{\partial x \partial z} + \frac{\partial^2 M_{zz}}{\partial z^2} + q = I_0 \frac{\partial^2 W_0}{\partial t^2} + I_1 \frac{\partial^2}{\partial t^2}\left(\frac{\partial U_0}{\partial x} + \frac{\partial V_0}{\partial z}\right)
\end{aligned} \tag{28}$$

In the above equations, (U_0, V_0, W_0) denote displacement along the coordinate lines of a material placed on x-z plane, q is the total transvers load and I_0, I_1 are the mass moments of inertia calculated as:

$$I_0 = \sum_{k=1}^{l} \rho^{(k)} (Y_{k+1} - Y_k) \tag{29}$$

$$I_1 = \frac{1}{2} \sum_{k=1}^{l} \rho^{(k)} (Y_{k+1}^2 - Y_k^2) \tag{30}$$

where $\rho^{(k)}$ is the density of the plate material at kth layer and Y represents thickness of each layer.

The in-plane force resultants (N_{xx}, N_{xz}, N_{zz}) and moment resultants (M_{xx}, M_{xz}, M_{zz}) are found, according to the equations below:

$$\begin{Bmatrix} N_{xx} \\ N_{zz} \\ N_{xz} \\ M_{xx} \\ M_{zz} \\ M_{xz} \end{Bmatrix} = \begin{bmatrix} A_{11} & A_{12} & A_{16} & B_{11} & B_{12} & B_{16} \\ A_{12} & A_{22} & A_{26} & B_{12} & B_{22} & B_{26} \\ A_{16} & A_{26} & A_{66} & B_{16} & B_{26} & B_{66} \\ B_{11} & B_{12} & B_{16} & D_{11} & D_{12} & D_{16} \\ B_{12} & B_{22} & B_{26} & D_{12} & D_{22} & D_{26} \\ B_{16} & B_{26} & B_{66} & D_{16} & D_{26} & D_{66} \end{bmatrix} \times \begin{Bmatrix} \varepsilon_{xx}^{(0)} \\ \varepsilon_{zz}^{(0)} \\ \gamma_{xz}^{(0)} \\ \varepsilon_{xx}^{(1)} \\ \varepsilon_{zz}^{(1)} \\ \gamma_{xz}^{(1)} \end{Bmatrix} \tag{31}$$

where:

$$A_{ij} = \sum_{k=1}^{l} \overline{Q}_{ij}^{(k)} (Y_{k+1} - Y_k) \ldots\ldots \text{i, j=1,2,6} \tag{32}$$

$$B_{ij} = \frac{1}{2} \sum_{k=1}^{l} \overline{Q}_{ij}^{(k)} (Y_{k+1}^2 - Y_k^2) \ldots\ldots \text{i, j=1,2,6} \tag{33}$$

$$D_{ij} = \frac{1}{3} \sum_{k=1}^{l} \overline{Q}_{ij}^{(k)} (Y_{k+1}^3 - Y_k^3) \ldots\ldots \text{i, j=1,2,6} \tag{34}$$

and:

$$\{\varepsilon^{(0)}\} = \begin{Bmatrix} \varepsilon_{xx}^{(0)} \\ \varepsilon_{zz}^{(0)} \\ \gamma_{xz}^{(0)} \end{Bmatrix} = \begin{Bmatrix} \partial U_0 / \partial x \\ \partial V_0 / \partial z \\ \partial U_0 / \partial z + \partial V_0 / \partial x \end{Bmatrix} \tag{35}$$

$$\{\varepsilon^{(1)}\} = \begin{Bmatrix} \varepsilon_{xx}^{(1)} \\ \varepsilon_{zz}^{(1)} \\ \gamma_{xz}^{(1)} \end{Bmatrix} = \begin{Bmatrix} -\partial^2 W_0 / \partial x^2 \\ -\partial^2 W_0 / \partial z^2 \\ -2\,\partial^2 W_0 / \partial x \partial z \end{Bmatrix} \tag{36}$$

A_{ij}, B_{ij} and D_{ij} are extensional, coupling, and bending stiffness, respectively; $\overline{Q}_{ij}^{(k)}$, a material constant, is the function of physical properties of each ply (kth), $\{\varepsilon^{(0)}\}$ is the membrane strain, and $\{\varepsilon^{(1)}\}$ is the flexural (bending) strain (Reddy, 2004).

3.4 Equations of Media Interfaces

As depicted in Figure 2, the porous layer is constrained by a laminated composite plate. The transverse and in-plane displacements in the neutral axis are given in the following:

$$W_t(x,t) = W_t^0 e^{j(\omega t - \xi_x x)} \tag{37}$$

$$W_p(x,t) = W_p^0 e^{j(\omega t - \xi_x x)} \tag{38}$$

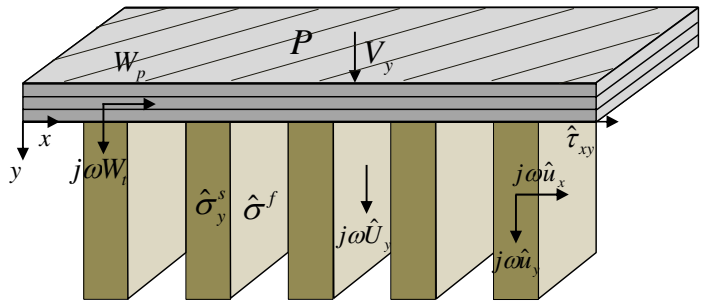

Figure 2: Detailed cross-sectional view of porous layer directly attached to a panel.

The elastic porous material is directly bonded to a panel, therefore, four BCs are obtained from the interface between the porous and composite layers (Bolton et al., 1996):

$$\hat{U}_y = W_t \tag{39}$$

$$\hat{u}_y = W_t \tag{40}$$

$$V_y = j\omega W_t \tag{41}$$

$$\hat{u}_x = W_p(\pm)(h_p / 2)(dW_t / dx) \tag{42}$$

In addition, the two other boundary conditions are obtained according to equation of motion in CLPT (Eq. 28), namely:

$$(\pm)\hat{\tau}_{xy} = (A_{11}^{(i)}\xi_x^2 - I_0^{(i)}\omega^2)W_P + (jB_{11}^{(i)}\xi_x^3 - jI_1^{(i)}\omega^2\xi_x)W_t \tag{43}$$

$$(\pm)P(\mp)(\hat{\sigma}^f + \hat{\sigma}_y^s) - j\xi_x(h_P / 2)\hat{\tau}_{xy} = (D_{11}^{(i)}\xi_x^4 - I_0^{(i)}\omega^2)W_t + (jI_1^{(i)}\omega^2\xi_x - jB_{11}^{(i)}\xi_x^3)W_p \tag{44}$$

In the above-mentioned equations, P denotes pressure in the exterior acoustics field at the interface, V_y stands for normal component of the particle velocity in the exterior medium at the interface, h_p is thickness of the panel, $I_0^{(i)}$ and $I_1^{(i)}$ are mass moments of inertia in the ith layer, $A_{11}^{(i)}$ represents extensional stiffness, $B_{11}^{(i)}$ represents bending-extensional coupling stiffness and $D_{11}^{(i)}$ denotes bending stiffness. In recent two BCs, the first signs are appropriate when the porous material is attached to the positive y (facing surface of the panel) and the second signs indicates that the porous material is attached to the negative y (facing surface).

3.5 TL Prediction

As previously depicted in Figure 1, thirteen types of wave branches are propagated into the double composite panel with a bounded porous layer. Meanwhile, twelve BCs presented in Eqs. (39-44), can be put into a matrix equation followed as:

$$[\hbar]_{12\times12}\{\lambda\}_{12\times1} = \{H\}_{12\times1} \tag{45}$$

$$\begin{bmatrix} \hbar_1 & 0 & 0 & 0 & 0 & 0 & 0 & 0 & \hbar_2 & 0 & 0 & 0 \\ 0 & \hbar_3 & \hbar_4 & \hbar_5 & \hbar_6 & \hbar_7 & \hbar_8 & 0 & \hbar_9 & 0 & 0 & 0 \\ 0 & \hbar_{10} & \hbar_{11} & \hbar_{12} & \hbar_{13} & \hbar_{14} & \hbar_{15} & 0 & \hbar_{16} & 0 & 0 & 0 \\ 0 & \hbar_{17} & \hbar_{18} & \hbar_{19} & \hbar_{20} & \hbar_{21} & \hbar_{22} & 0 & \hbar_{23} & \hbar_{24} & 0 & 0 \\ 0 & \hbar_{25} & \hbar_{26} & \hbar_{27} & \hbar_{28} & \hbar_{29} & \hbar_{30} & 0 & \hbar_{31} & \hbar_{32} & 0 & 0 \\ \hbar_{33} & \hbar_{34} & \hbar_{35} & \hbar_{36} & \hbar_{37} & \hbar_{38} & \hbar_{39} & 0 & \hbar_{40} & \hbar_{41} & 0 & 0 \\ 0 & 0 & 0 & 0 & 0 & 0 & 0 & \hbar_{42} & 0 & 0 & \hbar_{43} & 0 \\ 0 & \hbar_{44} & \hbar_{45} & \hbar_{46} & \hbar_{47} & \hbar_{48} & \hbar_{49} & 0 & 0 & 0 & \hbar_{50} & 0 \\ 0 & \hbar_{51} & \hbar_{52} & \hbar_{53} & \hbar_{54} & \hbar_{55} & \hbar_{56} & 0 & 0 & 0 & \hbar_{57} & 0 \\ 0 & \hbar_{58} & \hbar_{59} & \hbar_{60} & \hbar_{61} & \hbar_{62} & \hbar_{63} & 0 & 0 & 0 & \hbar_{64} & \hbar_{65} \\ 0 & \hbar_{66} & \hbar_{67} & \hbar_{68} & \hbar_{69} & \hbar_{70} & \hbar_{71} & 0 & 0 & 0 & \hbar_{72} & \hbar_{73} \\ 0 & \hbar_{74} & \hbar_{75} & \hbar_{76} & \hbar_{77} & \hbar_{78} & \hbar_{79} & \hbar_{80} & 0 & 0 & \hbar_{81} & \hbar_{82} \end{bmatrix} \times \begin{Bmatrix} p_{n1}^{R} \\ p_{n2}^{T1} \\ p_{n2}^{R1} \\ p_{n2}^{T2} \\ p_{n2}^{R2} \\ p_{n2}^{T3} \\ p_{n2}^{R3} \\ p_{n3}^{T} \\ w_{t1}^{0} \\ w_{p1}^{0} \\ w_{t2}^{0} \\ w_{p2}^{0} \end{Bmatrix} = \begin{Bmatrix} H_1 \\ 0 \\ 0 \\ 0 \\ 0 \\ H_2 \\ 0 \\ 0 \\ 0 \\ 0 \\ 0 \\ 0 \end{Bmatrix} \tag{46}$$

In the above equations, is a 12×12 coefficient matrix, $\{\lambda\}$ is a 12×1 vector showing the unknown parameters including pressure and displacement fields of the structure, and $\{H\}$ is a 12×1 vector representing the acoustic forces (the elements of matrix $[\hbar]$ and vector $\{H\}$ are listed in APPENDIX). These equations can be used to solve 12 unknown parameters including: p_{n1}^{R}, p_{n2}^{T1}, p_{n2}^{R1}, p_{n2}^{T2}, p_{n2}^{R2}, p_{n2}^{T3}, p_{n2}^{R3}, p_{n3}^{T}, w_{t1}^{0}, w_{p1}^{0}, w_{t2}^{0} and w_{p2}^{0} in terms of amplitude of the incident wave p_{n1}^{i}, frequency and incidence angle γ.

Noting that the transmission loss is not dependent on the incident wave, its amplitude is assumed to be unit. The transmission coefficient, $\tau_{(\gamma)}$, is the ratio of amplitudes of the incident and transmitted waves (p_{n3}^{T} / p_{n1}^{i}), which is obviously a function of the incidence angle γ. In practical applications, the incident wave is randomly impinged into the structure. Therefore, a practical parameter should be introduced to evaluate the experimental results. According to Paris formula, the averaged pressure transmission coefficient, $\bar{\tau}$, is calculated as below (Pierce, 1981):

$$\bar{\tau} = 2\int_0^{\gamma_m} \tau(\gamma)\sin\gamma\cos\gamma\, d\gamma \tag{47}$$

where γ_m is the maximum incident angle, varying between 70° and 85° (78° in this study) (Mulholland et al., 1967). The integration of Eq. (47) is conducted numerically by Simpson's rule and the average transmission loss (TL_{avg}) is finally obtained as below:

$$TL_{avg} = 10\log(\frac{1}{\tau}) \tag{48}$$

4 STATISTICAL ENERGY ANALYSIS

SEA method was first developed by Lyon (Lyon, 1956) and others in 1960's. Crocker et al. used SEA to predict the sound transmission of isotropic single-layered panels (Crocker and Price, 1969). In this section, the same theoretical model is used to predict the sound transmission loss for the double-walled composite panels by using AutoSEA2 software, according to ASTM E90. The subsystems and energy flow relationship are illustrated schematically in Figure 3. The source and the receiving rooms are the first and the third subsystems. Moreover, the composite panel lined with a layer of noise-control treatment is the second one. The external excitation has been generated by the diffuse source field located in the source room. Also, the foam module is based on Biot's theory of porous media. Therefore, the random incidence transmission loss measurement is developed in the software code AutoSEA2 (AutoSEA2 User's Guide, 2004).

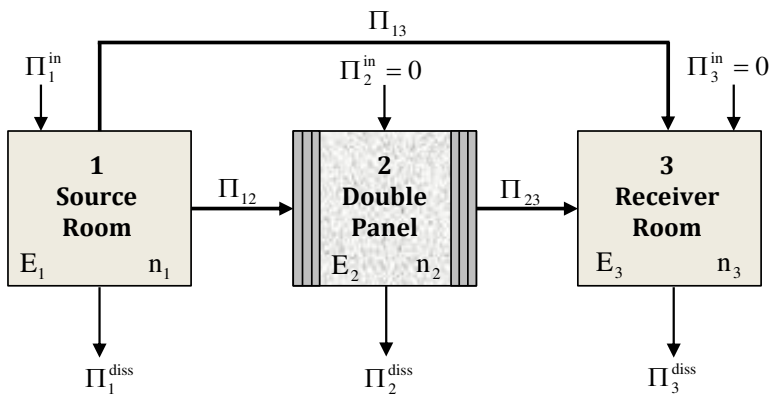

Figure 3: The flow of the power between the three sub-systems of double composite panel.

AutoSEA2 uses Statistical Energy Analysis (SEA) to analyze structural acoustic systems (AutoSEA2 User's Guide, 2004). The SEA model consists of two thin, simply supported plates separated by a porous layer. It is assumed that only out-of-plane waves are propagated. The double-panel is separating two adjacent 3D acoustic cavities. One of them is the source room while the second one is the receiver room. The source cavity resembles the reverberation room, while the receiver one is the anechoic chamber. The external excitation was generated by the diffuse source field located in the source room. The panel and the acoustic cavities were both connected by an SEA area junction. For the purpose of the energy flow analysis and prediction of the transmission loss, the SEA model was basically developed. The SEA double-panel lined with porous material model and acoustical area junction are illustrated in the Figure 4.

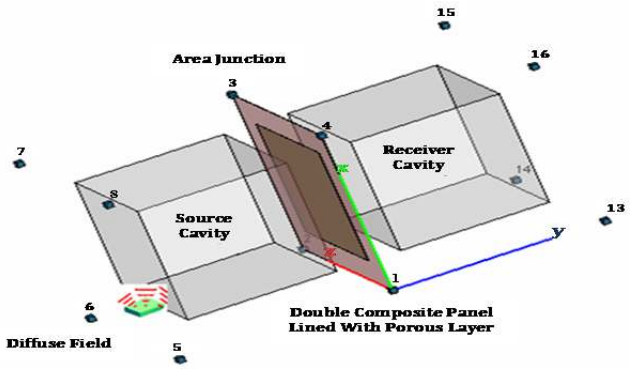

Figure 4: SEA model of double composite panel lined with elastic porous material.

If only the source room is excited using loudspeakers and there is no other power input to the other subsystems, then the power balance equations can be expressed as (Craik, 2003):

$$\Pi_{inc} = \frac{< P_1^2 >}{4\rho^* c} A_p \tag{49}$$

$$\Pi_{12} = \Pi_2^{diss} + \Pi_{23} \tag{50}$$

$$\Pi_{13} + \Pi_{23} = \Pi_3^{diss} \tag{51}$$

where , Π_i^{diss} and Π_{ij} are the power input to ith subsystem, the power dissipated in ith system and the power flow between subsystems i and j, respectively. These parameters can be written as below for each subsystem:

$$\Pi_i^{diss} = \omega E_i \eta_i \tag{52}$$

$$\Pi_{ij} = \omega \eta_{ij} n_i (\frac{E_i}{n_i} - \frac{E_j}{n_j}) \tag{53}$$

where ω is the angular frequency, n_i and n_j denote the modal densities of subsystems i and j, and finally, η_{ij} represents the coupling loss factor. The equation according to the reciprocity principle should be also satisfied (Craik, 2003).

Since the sound field of the source room is assumed to be reverberant, the energy stored, can be expressed by:

$$E_1 = \frac{< P_1^2 >}{\rho^* c^2} V_1 \tag{54}$$

$$\eta_{ij} / \eta_{ji} = n_j / n_i$$

$< P_1^2 >$ stands for average square sound pressure, V_1 is the volume, c is the speed within the cavity and ρ^* is surface density.

The mechanical energy stored in the panel is obtained as:

$$E_2 =< v^2 > \rho_s A_p \tag{55}$$

where v is the velocity, ρ_s and A_p are the surface density and the area of the panel, respectively.

Therefore, the sound transmission loss, TL, can be calculated by:

$$TL = 10\log(\frac{1}{\tau}) = 10\log(\frac{\Pi_{inc}}{\Pi_{23} + \Pi_{13}}) \tag{56}$$

where:

$$\Pi_{inc} = \frac{< P_1^2 >}{4\rho^* c} A_p \tag{57}$$

In the above equation, Π_{inc} is the sound power incident in the source room (Cremer and Heckl, 1988; Moore and Lyon, 1991).

5 RESULTS, COMPARISON AND DISCUSSION

The geometrical and environmental properties of the constituent layers are listed in Table 1. In addition, each layer of the laminated composite panel is made of graphite (T300/5208)/epoxy (properties of the composite layers are summarized in Table 2), where the plies are arranged in a $\left[90°, 0°, 90°, 0°\right]_s$ pattern.

Parameters	Symbol	Unit	Incident (1)	Panel (2)			Transmitted (3)
				Excited Panel	Porous Layer	Radiating panel	
Material	-----	-----	Air	Composite	Polyurethane	Composite	Air
Density	ρ_a	Kg/m^3	1.21	-----	-----	-----	1.21
Speed of sound	c	ms^{-1}	342	-----	-----	-----	342
Thickness	h	mm	-----	1	20	1	-----
Porosity	φ	-----	-----	-----	0.9	-----	-----
Flow resistivity	σ_r	Nm^{-4}s	-----	-----	25e3	-----	-----
Tortuosity	α_∞	-----	-----	-----	7.8	-----	-----
Viscous charact.	Λ	µm	-----	-----	226	-----	-----
Thermal charact.	Λ'	µm	-----	-----	226	-----	-----
Bulk density of solid phase	ρ_1	Kg/m^3	-----	-----	30	-----	-----
Bulk Young's Modulus	E	Pa	-----	-----	8e5	-----	-----
Shear Modulus	δ	Pa	-----	-----	2.86e5	-----	-----
Bulk Poisson coefficient	ν	-----	-----	-----	0.4	-----	-----
Structural Damping	-----	-----	-----	-----	0.265	-----	-----

Table 1: Geometrical and environmental properties (Bolton et al., 1996; Lee et al., 2001).

Material	E_x (GPa)	E_z (GPa)	G_{xz} (GPa)	υ_{xz}	Density (Kg/m^3)
Aluminum	70	70	26.3	0.33	2700
Glass/Epoxy	38.6	8.27	4.14	0.26	1900
Graphite(T300/5208)/Epoxy	181	10.3	7.17	0.28	1600
Kevlar49/Epoxy	76	5.5	2.3	0.34	1460

Table 2: Orthotropic properties (Vinson and Sierakowski, 2002)

Also, the dimensions and physical properties of each subsystem of SEA model are listed in Table 3.

Subsystems	Dimensions		Material	Technical Data
Source Room	1.2 x 1.2 x 1.2 m		Air	Damping Loss Factor = 0.1 % Table (1)
Double Composite Panel Lined with Porous Material	1.2 x 1.2 x	Excited Panel 0.001 m	Graphite(T300/5208)/Epoxy	Table (2)
		Foam Layer 0.02 m	Polyurethane	Table (1)
		Radiating Panel 0.001 m	Graphite(T300/5208)/Epoxy	Table (2)
Receiving Room	1.2 x 1.2 x 1.2 m		Air	Absorption Coefficient = 100 % Table (1)

Table 3: Dimensions and physical properties of three subsystems of SEA model.

The transmission loss of the structure, as a designing parameter, is predicted using analytical and SEA models. Then, the effects of physical parameters as well as boundary conditions are investigated.

5.1 Associated Parameters of SEA Model

The modal density, coupling loss factor and radiation efficiency give the basic parameters required for the SEA model. The accuracy of the prediction of the response is greatly dependent on the following two conditions:

1. The Statistical Energy Analysis requires a sufficiently high modal density.
2. The coupling loss factor between subsystems is small in comparing with corresponding internal loss factor. In other words, the subsystems are weakly coupled to each other.

The modal density represents the number of resonance modes that have the ability to receive and store the energy in a subsystem and it does not depend on the boundary conditions (Beranek and Ver, 1992). Figure 5 shows the number of modes in a band for all three subsystems. It can be seen that the number of modes are significantly great at high frequencies. This is happened more rapidly in both of the cavities instead of the panel.

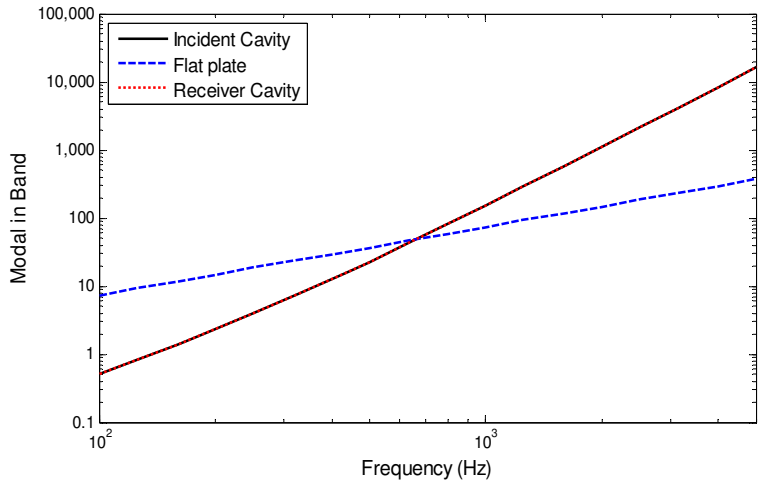

Figure 5: The number of modes in a band for three subsystems.

On the other hand, according to Figure 6 internal loss factor between subsystems in this model, especially at the high frequencies, is much larger than the coupling loss factor. In other words, the subsystems are weakly coupled to each other.

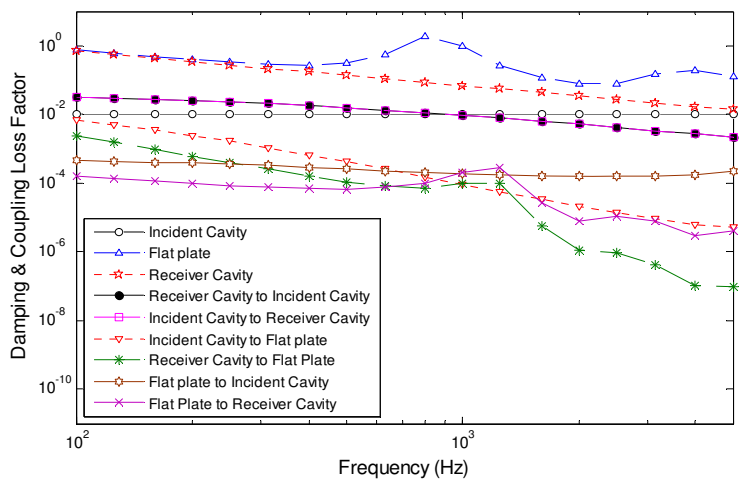

Figure 6: Comparison between damping loss factors and coupling loss factors among all SEA model subsystems.

Thus, through the descriptions noted above, the SEA model presented here is reliable, especially in high frequency ranges.

5.2 Validation

Figure 7 demonstrates theoretical predictions and SEA method as well as experimental results from Ref. (Bolton et al., 1996) for a double composite panel lined with a foam layer for a special case of isotropic materials. In other words, the mechanical properties of lamina in all directions of present work are chosen to be the same as those of an isotropic material such as Aluminum. Then, the fiber angles would approach zero. It is obvious that there is an excellent agreement between analytical, experimental and simulation results.

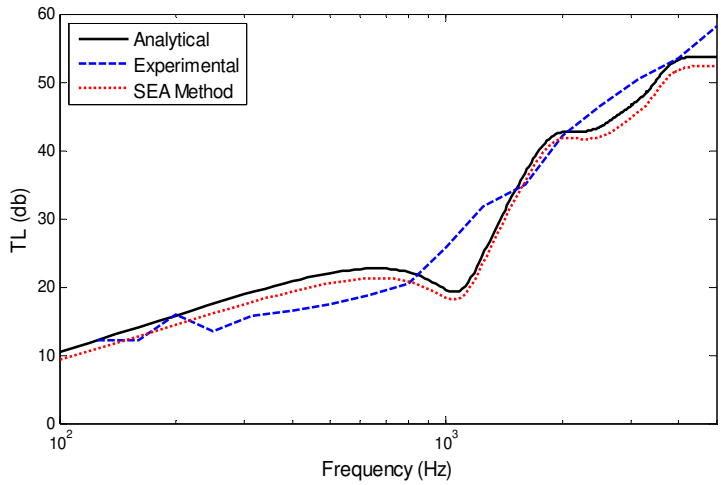

Figure 7: Comparison between the analytical method, experimental results and SEA model for a double panel lined with porous media.

Figure 8 compares the TL values of the laminated composite walls obtained from the present model and SEA method, where each layer of the laminated composite panels is made up of graphite (T300/5208)/epoxy with the plies being arranged in a $\left[90°, 0°, 90°, 0°\right]_s$ pattern. The results show an excellent agreement.

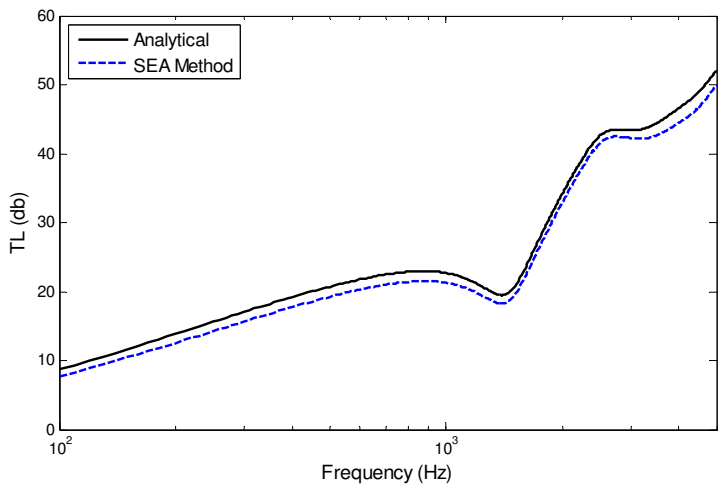

Figure 8: Comparison of SEA and analytical model for a double composite panel.

5.3 The Effect of Parameters on Structural TL

To study the effect of the porous layer on the TL, a composite panel with/without the intermediate porous layer is considered. Meanwhile, those panels are compared with a double-walled composite panel lined with a porous layer. As depicted in Figure 9, the results of the TL for double composite panel are significantly enhanced especially at high frequencies.

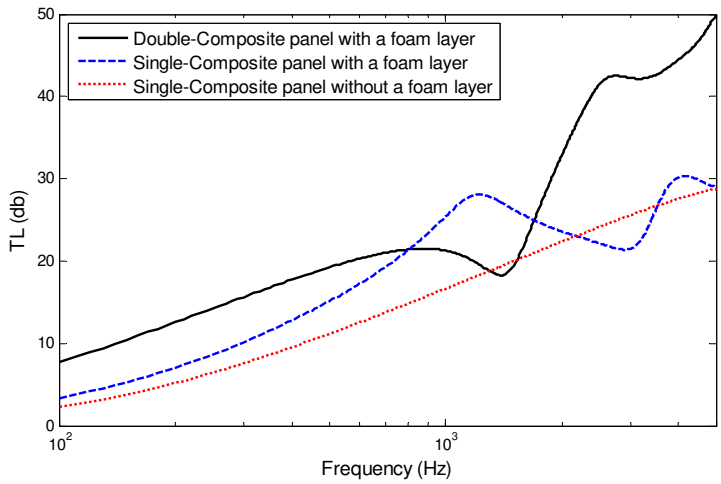

Figure 9: TL of the single panel, single panel lined with foam and double panel lined with foam.

As the porous material plays an important role on TL, then the sensitivity of TL to parameters of porous layers should be considered. These parameters are distributed into three categories:

1. Thickness of the porous layer
2. Parameters associated with the fluid phase of the porous layer which include: Porosity, Tortuosity and Flow Resistivity.
3. Parameters related to the solid phase of the porous layer which involve: Bulk Density, Bulk Young's Modulus and Poisson's Ratio.

As illustrated in Figure 10, due to thickening of the porous layer, a considerable increase in the TL is obtained.

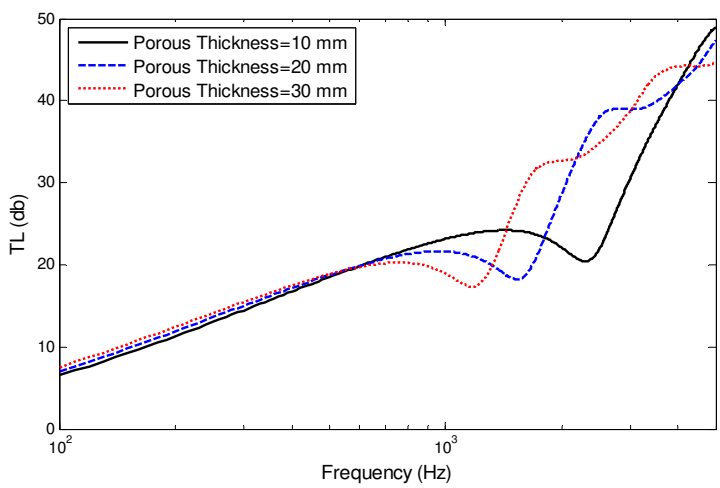

Figure 10: Comparison of a double composite panel lined with porous material with different porous layer thickness.

Therefore, a significant attention should be devoted to thickness of porous layer, as it plays a key role in noise attenuation especially at high frequencies. It should be also noted that increasing the thickness may lead to reduction of the coincidence frequency.

The parameters associated with fluid phase of porous material are considered in Figure 11. As depicted in this figure, with considering the variety of the flow resistivity, porosity and tortuosity into the present model, the corresponding TL's are not effectively changed. It is due to the fact that the air-borne noise cannot be able to carry the energy in this configuration.

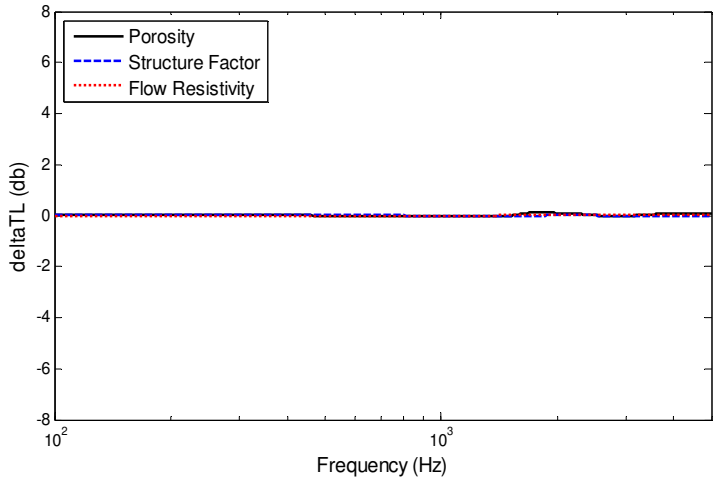

Figure 11: Sensitivity of the parameters associated with the fluid phase of the porous layer ($\varphi = 0.9, 0.99;\ \alpha_\infty = 7.8, 10;\ \sigma_r = 25000, 31500$).

In addition, Figure 12 shows the effect of parameters related to solid phase of the porous layer such as bulk density, bulk Young's modulus and Poisson's ratio, on TL of the double-walled composite panel. It is well observed that, these parameters can effectively change the TL especially in high frequency range. In other word, it appears that the frame wave is the major energy carrier in this configuration.

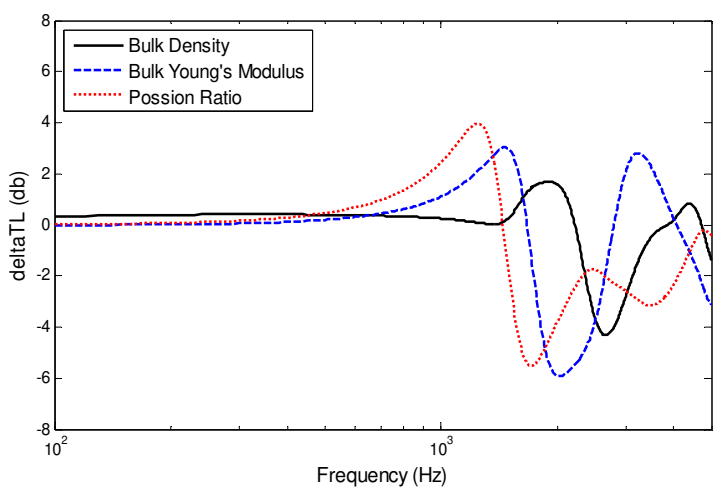

Figure 12: Sensitivity of the parameters associated with the solid phase of the porous layer ($\rho_1 = 30, 40$ Kg/m^3; $E = 8\times10^5, 1.5\times10^6$ Pa; $\nu = 0.3, 0.4$).

Moreover, Table 4 shows the influence of corresponding parameters of the solid phase of the porous layer such as bulk density, bulk Young's modulus and Poisson's ratio on TL. As listed in the Table:

1. In low frequency ranges, increasing the bulk density improves the TL. However, in high frequencies it significantly reduces the TL.
2. Reducing the bulk Young's modulus of the foam has a more significant effect on improvement of the TL in the structure at frequencies above 1000 Hz but exactly an opposite case occurs at low frequency ranges. It should be noted that decreasing the bulk Young's modulus increases frequency of the coincidence resonance.
3. In spite of the fact that Poisson's ratio has no effect in lower frequencies, the TL will be enhanced by decreasing the Poisson's ratio in high frequencies.

		Frequency (Hz)								
		100	200	400	800	1000	2000	3000	4000	5000
TL (db)	Bulk Density (ρ_1) = 10 Kg/m^3	6.36	11.04	16.28	20.56	21.06	26.07	42.72	52.71	57.06
	ρ_1 = 30 Kg/m^3	7.03	11.9	17.16	21.3	21.62	28.7	38.94	41.96	47.33
	ρ_1 = 90 Kg/m^3	8.86	14.03	19.33	23	22.83	26.07	37.28	38.42	40.2
Error (%) (in comparison to ρ_1 = 10 Kg/m^3)		11%	8%	5%	4%	3%	10%	-9%	-20%	-17%
		39%	27%	19%	12%	8%	0%	-13%	-27%	-30%
TL (db)	Bulk Young's Modulus (E) = 1e5 Pa	6.92	11.34	14.58	16.55	22.67	43.58	47.61	48.1	57.77
	E = 4e5 Pa	7.02	11.8	16.71	18.89	17.13	33.14	41.57	46.18	45.05
	E = 8e5 Pa	7.03	11.9	17.16	21.3	21.62	28.7	38.94	41.96	47.33
Error (%) (in comparison to E = 1e5 Pa)		1%	4%	15%	14%	-24%	-24%	-13%	-4%	-22%
		2%	5%	18%	29%	-5%	-34%	-18%	-13%	-18%
TL (db)	Possion's Ratio (ν) = 0.3	7.01	11.82	16.87	19.93	19.17	32.48	41.5	44.28	47.74
	ν = 0.4	7.03	11.9	17.16	21.3	21.62	28.7	38.94	41.96	47.33
	ν = 0.48	7.05	11.98	17.54	23	24.47	26.06	37.47	38	41.46
Error (%) (in comparison to ν = 0.3)		0%	1%	2%	7%	13%	-12%	-6%	-5%	-1%
		1%	1%	4%	15%	28%	-20%	-10%	-14%	-13%

Table 4: Comparison the influence of corresponding parameters of the solid phase of the porous layer on TL.

Thickness of the composite panels is one of the most efficient parameters in noise transfer; therefore according to Figure 13, the influence of this parameter on transmission loss is examined. It is observed that in all frequency ranges, increasing the thickness of the panel will enhance the TL coefficient. In other words, sound waves which pass through the thicker walls are less spread and more reflective.

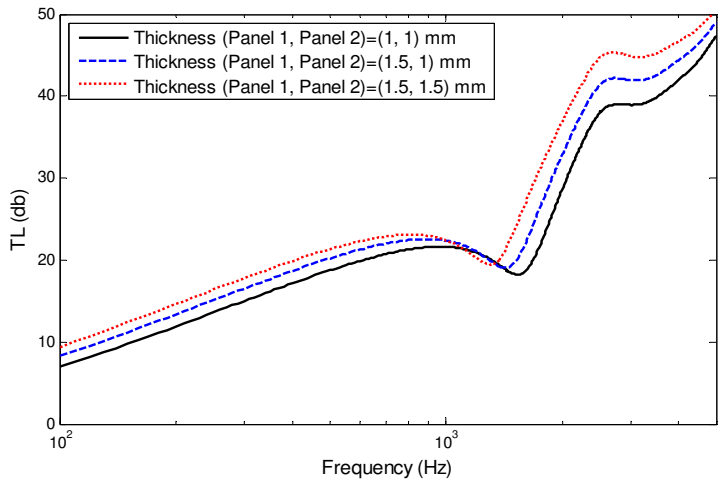

Figure 13: The effect of thickness of composite panels on TL.

The effect of composite materials on TL has been shown in Figure 14. The materials chosen for such comparison are Graphite (T300/5208)/epoxy, Kevlar49/epoxy and Glass/epoxy (see Table 2). The figure shows that the material must be chosen properly to enhance the TL in a broad band frequency. The results represent a desirable level of TL for the Graphite (T300/5208)/epoxy. It is readily seen that, as a result of the density of the materials, the TL curves are ascending. Hence, the Glass/epoxy material demonstrates a better transmission loss due to the density that is greater than the other two materials.

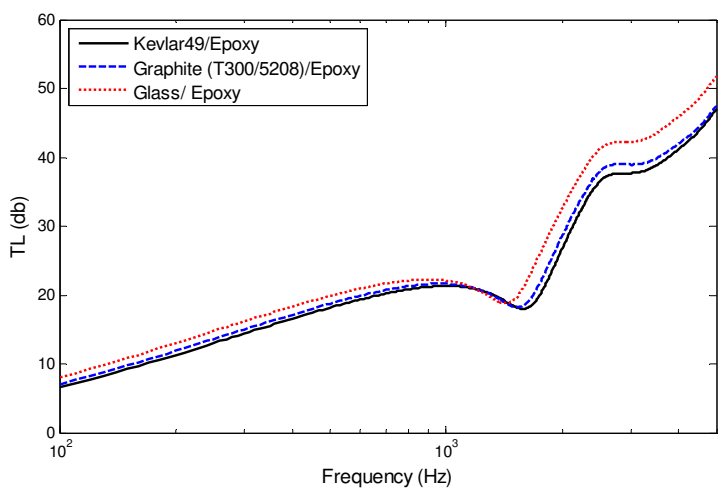

Figure 14: The effect of composite material on TL.

Figure 15 illustrates the effect of stacking sequence. Three patterns $\left[0°,0°,0°,0°\right]_s$, $\left[0°,90°,0°,90°\right]_s$, $\left[90°,0°,90°,0°\right]_s$ and $\left[90°,90°,90°,90°\right]_s$ are defined to designate stacking sequence of the plies. As shown the plies arrangement $\left[90°,90°,90°,90°\right]_s$ has enhanced the structural TL more than the other options, particularly at higher frequencies.

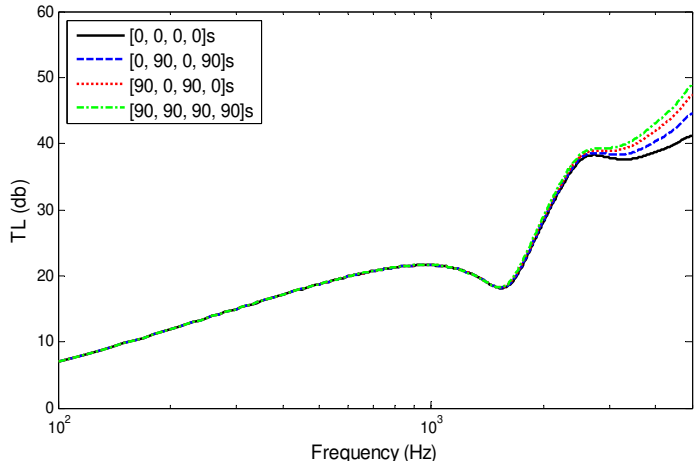

Figure 15: The effect of the composite plies arrangement in TL.

6 CONCLUSIONS

An analytical model of sound transmission was described in this paper for the double-walled composite panels lined with a porous medium. First of all, the governing equations of wave propagation within porous materials were extracted using Biot's theory as well as stress-strain relations. Then, the governing equations of layered composite panels were used based on CLPT. Finally, the TL was obtained with the aid of the equations applied to boundary conditions.

Furthermore, the acoustic behavior of this structure was analyzed using SEA method by separating the system of the double-walled porous composite panel into three sub-systems. In order to verify the results, TL coefficients of the structure via SEA was compared with those obtained from the presented analytical model as well as experimental measurements. The comparison reveals an excellent agreement. However, the accuracy of the results was more satisfied at high frequencies due to the statistical nature of the SEA technique.

At last, the influences of effective parameters were studied on TL of sound in these structures. The results showed that using the double-walled composite panels lined with a porous layer leads into the weight reduction as well as providing a better performance as compared to the single-walled composite panels especially at high frequencies. Meanwhile, investigation of the sensitivity of the related parameters with the porous layer on sound performance of the structure showed that when the porous later is bonded between two plates, the maximum sound energy is transferred by the frame waves. Therefore, the associated parameters of the solid phase (frame) such as modulus of elasticity and bulk density will have the greatest effect on the TL coefficient. Finally, it can be concluded that the composite material along with layer stacking sequence of the composite plies is more effective on TL, especially in high frequency ranges.

References

Biot, M. A., (1956). Theory of propagation of elastic waves in a fluid-structural porous solid I: Low frequency range. Journal of the Acoustical Society of America 28(2): 168-178.

Bolton, J. S. and Green, E. R., (1993). Normal incidence sound transmission through double-panel systems lined with relatively stiff, partially reticulated polyurethane foam. Applied Acoustics 39(1–2): 23-51.

Bolton, J. S., Heng, Y. L., katragadda, S. and Alexander, J. H., (1997). Layered fibrous treatment for a sound absorption and transmission control. SAE 971878: 2576-2590.

Bolton, J. S., Shiau, N. M. and Kang, Y. J., (1996). Sound transmission through multi-panel structures lined with elastic porous materials. Journal of Sound and Vibration 191(3): 317-347.

Allard, J. F. and Atalla, N., (2009). Propagation of sound in porous media modelling sound absorbing materials. Wiley (Chichester, West Sussex, U.K.).

Cimerman, B., Bremner, P., Yang, Qian and Van Buskirk, J. A., (1995). Incorporating layered acoustic trim materials in body structural-acoustic models. SAE 951307: 2289-2294.

Zeng, X., Woo, J. and Tang, H., (2002). The effects of laminated steel body panels on vehicle interior noise. Proceedings of the second International Auto SEA Users Conference. (Michigan).

Tadeu, A., Antonio, J. and Mateus, D., (2004). Sound insulation provided by single and double panel walls-a comparison of analytical solutions versus experimental results. Applied Acoustics 65(1): 15-29.

Onsay, T., (2007). Use of sea in a car program. SAE Noise and Vibration Conference. (USA).

Ghosh, A. K., Williams, A. D., Zucker, J. M., Mathews J. L. and Spinhirne, N., (2008). An experimental investigation into the acoustic characteristics of fluid-filled porous structures-a simplified model of the human skull cancellous structure. Experimental Mechanics 48(2): 139-152.

Xin, F. X., Lu, T. J. and Chen, C. Q., (2008). Vibroacoustic behavior of clamp mounted double-panel partition with enclosure air cavity. The Journal of the Acoustical Society of America 124(6): 3604-3612.

Xin, F. X. and Lu, T. J., (2011). Transmission loss of orthogonally rib-stiffened double-panel structures with cavity absorption. The Journal of the Acoustical Society of America 129(4): 1919-1934.

Daneshjou, K., Ramezani, H. and Talebitooti, R., (2011). Wave transmission through laminated composite double-walled cylindrical shell lined with porous materials. Applied Mathematics and Mechanics 32(6): 701-718.

Lee, J. H., Kim, J. and Kim, H. J., (2001). Simplified method to solve sound transmission through structures lined with elastic porous material. The Journal of the Acoustical Society of America 110(5): 2282-2294.

Reddy, J. N., (2004). Mechanics of laminated composite plates and shells: theory and analysis. CRC Press (Boca Raton).

Pierce, A. D., (1981). Acoustics: An introduction to its physical principles and applications. McGraw-Hill Book Co.

Mulholland, K. A., Parbrook, H. D. and Cummings, A., (1967). The transmission loss of double panels. Journal of Sound and Vibration 6(3): 324-334.

Lyon, R. H., (1956). Propagation of correlation functions in continuous media. The Journal of the Acoustical Society of America 28(1): 76-79.

Crocker, M. J. and Price, A. J., (1969). Sound transmission using statistical energy analysis. Journal of Sound and Vibration 9(3): 469-486.

AutoSEA2 user's guide (2004). ESI Group.

Craik, R. J. M., (2003). Non-resonant sound transmission through double walls using statistical energy analysis. Applied Acoustics 64(3): 325-341.

Cremer, L. and Heckl, M., (1988). Structure-borne sound: Structural vibrations and sound radiation at audio frequencies. Springer-Verlag (Berlin; New York).

Moore, J. A. and Lyon, R. H., (1991). Sound transmission loss characteristics of sandwich panel constructions. The Journal of the Acoustical Society of America 89(2): 777-791.

Vinson, J. R. and Sierakowski, R. L., (2002). The behavior of structures composed of composite materials. Springer.

Beranek, L. L. and Ver, I. L., (1992). Noise and vibration control engineering principles and application. Wiley-Interscience.

APPENDIX

The non-zero elements of the matrix $[\hbar]$ appearing in Eq. (46) are followed as:

$$
\begin{aligned}
\hbar_1 &= \xi_y \\
\hbar_2 &= \omega \\
\hbar_3 &= \Psi(\alpha) \\
\hbar_4 &= -\Psi(\alpha) \\
\hbar_5 &= \Psi(\beta) \\
\hbar_6 &= -\Psi(\beta) \\
\hbar_7 &= \Psi'(4) \\
\hbar_8 &= \Psi'(4) \\
\hbar_9 &= j \\
\hbar_{10} &= b_1\Psi(\alpha) \\
\hbar_{11} &= -b_1\Psi(\alpha) \\
\hbar_{12} &= b_2\Psi(\beta) \\
\hbar_{13} &= -b_2\Psi(\beta) \\
\hbar_{14} &= g\Psi'(4) \\
\hbar_{15} &= g\Psi'(4) \\
\hbar_{16} &= j \\
\hbar_{17} &= \Psi'(\alpha) \\
\hbar_{18} &= \Psi'(\alpha) \\
\hbar_{19} &= \Psi'(\beta) \\
\hbar_{20} &= \Psi'(\beta) \\
\hbar_{21} &= -\Psi(4) \\
\hbar_{22} &= \Psi(4) \\
\hbar_{23} &= -\xi_x(h_{p1}/2) \\
\hbar_{24} &= j \\
\hbar_{25} &= 2N\xi_x\Psi(\alpha) \\
\hbar_{26} &= -2N\xi_x\Psi(\alpha)
\end{aligned}
\tag{A-1}
$$

$$
\begin{aligned}
\hbar_{27} &= 2N\xi_x\Psi(\beta)\\
\hbar_{28} &= -2N\xi_x\Psi(\beta)\\
\hbar_{29} &= N\left(\xi_x\Psi'(4)-\xi_{4y}\Psi(4)\right)\\
\hbar_{30} &= N\left(\xi_x\Psi'(4)-\xi_{4y}\Psi(4)\right)\\
\hbar_{31} &= (jI_1^{(1)}\omega^2\xi_x - jB_{11}^{(1)}\xi_x^3)\\
\hbar_{32} &= (I_0^{(1)}\omega^2 - A_{11}^{(1)}\xi_x^2)\\
\hbar_{33} &= j\omega\rho_0\\
\hbar_{34} &= \Omega(h_{p1},\alpha,1)\\
\hbar_{35} &= \Omega'(h_{p1},\alpha,1)\\
\hbar_{36} &= \Omega(h_{p1},\beta,2)\\
\hbar_{37} &= \Omega'(h_{p1},\beta,2)\\
\hbar_{38} &= \Omega''(h_{p1},2)\\
\hbar_{39} &= -\Omega''(h_{p1},1)\\
\hbar_{40} &= -D_{11}^{(1)}\xi_x^4 + I_0^{(1)}\omega^2\\
\hbar_{41} &= jB_{11}^{(1)}\xi_x^3 - jI_1^{(1)}\omega^2\xi_x\\
\hbar_{42} &= -\xi_y e^{-j\xi_y h_{foam}}\\
\hbar_{43} &= \omega\\
\hbar_{44} &= \Psi(\alpha)\Gamma(\alpha)\\
\hbar_{45} &= -\Psi(\alpha)\Gamma'(\alpha)\\
\hbar_{46} &= \Psi(\beta)\Gamma(\beta)\\
\hbar_{47} &= -\Psi(\beta)\Gamma'(\beta)\\
\hbar_{48} &= \Psi'(4)\Gamma(4)\\
\hbar_{49} &= \Psi'(4)\Gamma'(4)\\
\hbar_{50} &= j\\
\hbar_{51} &= b_1\Psi(\alpha)\Gamma(\alpha)\\
\hbar_{52} &= -b_1\Psi(\alpha)\Gamma'(\alpha)\\
\hbar_{53} &= b_2\Psi(\beta)\Gamma(\beta)\\
\hbar_{54} &= -b_2\Psi(\beta)\Gamma'(\beta)\\
\hbar_{55} &= g\Psi'(4)\Gamma(4)\\
\hbar_{56} &= g\Psi'(4)\Gamma'(4)\\
\hbar_{57} &= j\\
\hbar_{58} &= \Psi'(\alpha)\Gamma(\alpha)\\
\hbar_{59} &= \Psi'(\alpha)\Gamma'(\alpha)
\end{aligned}
\tag{A-1}
$$

$$
\begin{aligned}
\hbar_{60} &= \Psi'(\beta)\Gamma(\beta)\\
\hbar_{61} &= \Psi'(\beta)\Gamma'(\beta)\\
\hbar_{62} &= -\Psi(4)\Gamma(4)\\
\hbar_{63} &= \Psi(4)\Gamma'(4)\\
\hbar_{64} &= -\xi_x(h_{p2}/2)\\
\hbar_{65} &= j\\
\hbar_{66} &= 2\xi_x\Psi(\alpha)\Gamma(\alpha)\\
\hbar_{67} &= -2\xi_x\Psi(\alpha)\Gamma'(\alpha)\\
\hbar_{68} &= 2\xi_x\Psi(\beta)\Gamma(\beta)\\
\hbar_{69} &= -2\xi_x\Psi(\beta)\Gamma'(\beta)\\
\hbar_{70} &= [\xi_x\Psi'(4) - \xi_{4y}\Psi(4)]\Gamma(4)\\
\hbar_{71} &= [\xi_x\Psi'(4) - \xi_{4y}\Psi(4)]\Gamma'(4)\\
\hbar_{72} &= (jB_{11}^{(2)}\xi_x^3 - jI_1^{(2)}\omega^2\xi_x)\ /\ N\\
\hbar_{73} &= (A_{11}^{(2)}\xi_x^2 - I_0^{(2)}\omega^2)\ /\ N\\
\hbar_{74} &= \Omega'(h_{p2},\alpha,1)\Gamma(\alpha)\\
\hbar_{75} &= \Omega(h_{p2},\alpha,1)\Gamma'(\alpha)\\
\hbar_{76} &= \Omega'(h_{p2},\beta,2)\Gamma(\beta)\\
\hbar_{77} &= \Omega(h_{p2},\beta,2)\Gamma'(\beta)\\
\hbar_{78} &= \Omega''(h_{p2},1)\Gamma(4)\\
\hbar_{79} &= -\Omega''(h_{p2},2)\Gamma'(4)\\
\hbar_{80} &= j\omega\rho_0\\
\hbar_{81} &= D_{11}^{(2)}\xi_x^4 - I_0^{(2)}\omega^2\\
\hbar_{82} &= -jB_{11}^{(2)}\xi_x^3 + jI_1^{(2)}\omega^2\xi_x
\end{aligned}
\tag{A-1}
$$

$\{H\}$ Matrix elements include:

$$
H_1 = \xi_y \quad , \quad H_2 = -j\omega\rho_0 \tag{A-2}
$$

Assuming that:

$$\Psi(i) = \xi_{iy} \Big/ \xi_i^2 \ , \ \Psi'(i) = \xi_x \Big/ \xi_i^2 \qquad @\ i = \alpha, \beta, 4$$

$$\Gamma(i) = e^{-j\,\xi_{iy}\,h_{foam}} \ , \ \Gamma'(i) = e^{j\,\xi_{iy}\,h_{foam}} \qquad @\ i = \alpha, \beta, 4$$

$$\Omega(x,i,k) = \delta\,\Psi(i)[2\,\xi_{iy} - j\xi_x^2\,x] + A + \chi + b_k G \qquad @\ x = h_{p1}, h_{p2} \ ;\ i = \alpha, \beta \ ; \tag{A-3}$$

$$\Omega'(x,i,k) = \delta\,\Psi(i)[2\,\xi_{iy} + j\xi_x^2\,x] + A + \chi + b_k G \quad @\ x = h_{p1}, h_{p2} \ ;\ i = \alpha, \beta \ ;\ k$$

$$\Omega''(x,i) = \delta\,\Psi'(4)[2\xi_{4y} - (-1)^i\,jx(\xi_x^2 - \xi_{4y}^2) \Big/ 2] \qquad @\, x = h_{p1}, h_{p2} \ ; \quad i = 1,2$$

where:

$$A = \frac{\nu\ E}{(1+\nu)(1-2\nu)}$$

$$\delta = \frac{E}{2(1+\nu)}$$

$$g = -\hat{\rho}_{12}\ /\ \hat{\rho}_{22}$$

$$b_1 = \frac{\hat{\rho}_{11} - \hat{\rho}_{12}\chi}{\hat{\rho}_{22}\chi - \hat{\rho}_{12}\mu} - \frac{\phi\mu - \chi^2}{\omega^2(\hat{\rho}_{22}\chi - \hat{\rho}_{12}\mu)}\,\xi_\alpha{}^2 \tag{A-4}$$

$$b_2 = \frac{\hat{\rho}_{11} - \hat{\rho}_{12}\chi}{\hat{\rho}_{22}\chi - \hat{\rho}_{12}\mu} - \frac{\phi\mu - \chi^2}{\omega^2(\hat{\rho}_{22}\chi - \hat{\rho}_{12}\mu)}\,\xi_\beta{}^2$$

$$G = \rho_0\,c_2^2 \left\{ 1 + \frac{(\varsigma - 1)\sqrt{\varphi\sigma_r}}{\Pr^{\frac{1}{2}}\sqrt{-2j\omega\rho_0\alpha_\infty}}\,\frac{j_1\left(2\,\Pr^{\frac{1}{2}}\sqrt{\dfrac{-2j\omega\rho_0\alpha_\infty}{\varphi\sigma_r}}\right)}{j_0\left(2\,\Pr^{\frac{1}{2}}\sqrt{\dfrac{-2j\omega\rho_0\alpha_\infty}{\varphi\sigma_r}}\right)} \right\}^{-1} .$$